



Zn diffusion depth effect on photoresponse uniformity in InP/InGaAs avalanche photodiodes

A. W. Walker¹ · S. Moisa¹ · A. J. Springthorpe¹ · O. J. Pitts¹

Received: 28 October 2021 / Accepted: 19 May 2022 / Published online: 28 July 2022
© Crown 2022

Abstract

Numerical simulation of the electric field distribution and photocurrent response of a planar InP/InGaAs avalanche photodiode is presented for small variations of the multiplication width. The Zn dopant diffusion front is obtained by numerically simulating the diffusion process. The simulation results indicate that while a local peak value of the electric field is observed near the device edge, it is not associated with a significant increase in the photocurrent response. Experimental photocurrent mapping of an avalanche photodiode shows a response at the edge that is enhanced by ~60% compared to the centre response. Scanning electron microscope images of Zn diffused structures show that the depth is enhanced by 0.03 μm at the edge, compared to the centre. Simulations of devices with varied multiplication width show that the magnitude of the increase in photocurrent expected for the observed depth enhancement is consistent with the observed photocurrent enhancement along the edge the active device.

Keywords Avalanche photodetector · Breakdown · Numerical simulation · Multiplication width · Mask loading · Zn diffusion · InP · InGaAs

1 Introduction

Planar InP/InGaAs avalanche photodiodes (APDs) are in wide use in linear mode in optical communication systems and for single photon detection when operated in Geiger mode. A key design consideration is suppression of the edge breakdown effect, which leads to a lowering of the breakdown voltage and non-uniformity of the detector response both in linear mode (Burm et al. 2004) and in Geiger mode (Theocharous et al. 2010). Methods that have been developed to suppress edge breakdown, including the

This article is part of the Topical Collection on Numerical Simulation of Optoelectronic Devices.

Guest edited by Slawek Sujecki, Asghar Asgari, Donati Silvano, Karin Hinzer, Weida Hu, Piotr Martyniuk, Alex Walker and Pengyan Wen.

✉ A. W. Walker
alexandre.walker@nrc-cnrc.gc.ca

¹ Advanced Electronics and Photonics Research Centre, National Research Council of Canada, 1200 Montreal Road, M50, Ottawa, ON K1A 0R6, Canada

double diffusion method (Liu et al. 1992; Wei et al. 2002), and the recess etch method (Burm et al. 2004; Cho et al. 2000; Li et al. 2012), rely on creating a stepped diffusion profile with a shallower diffused outer region surrounding a deeper diffused central region. In such a stepped profile, the reduced electric field due to the increased multiplication width (MW) in the shallower diffused outer region is intended to counteract the enhancement of the field due to the junction curvature at the device edge. Numerical simulation (Haralson et al. 1997; Anti et al. 2012) and experimental measurements (Theocharous et al. 2010; Tosi et al. 2010) have shown that edge field enhancement effects may nonetheless occur, either at the edge of the deep diffused central region or at the edge of the shallow diffused region.

Experimental characterization of edge breakdown effects typically relies on raster scanning of the detector response in one or two dimensions with a focused beam (Burm et al. 2004; Theocharous et al. 2010). Previous investigations using numerical simulation have revealed localized enhancement of the electric field near the device edge due to the junction curvature (Vasileuski et al. 2008; Park et al. 2018), but did not simulate the photocurrent response specifically. Additionally, these works assumed either a constant Zn doping concentration (Vasileuski et al. 2008) or an error function profile (Park et al. 2018), neither of which corresponds closely to the actual diffusion profile. A previous work that reported numerical simulation of the APD photocurrent response (Xiao et al. 2008) assumed a constant value of the Zn doping level, and suggested this could be improved by employing the actual Zn diffusion profile. The observed enhancement of the photocurrent at the device edge for planar APDs has been generally attributed to the junction curvature effect in previous works (Burm et al. 2004; Theocharous et al. 2010).

Recently it has been shown experimentally that areas of enhanced photocurrent response are associated with increased Zn diffusion depth near the device edge in certain cases (Pitts, et al. 2020). The results reported in Pitts, et al. (2020) were obtained for APDs processed with a selective area growth-based process. It is of interest to consider whether similar effects are present in standard Zn diffusion processing. Comparison of large-area and masked Zn diffusion (Pitts et al. 2012) showed that the mask enhances the diffusion depth by approximately 30% compared to the large-area value, demonstrating the presence of a mask loading effect. Although this previous result, as well as, by analogy, the well-known growth rate enhancement effect observed in selective area growth (Sugiyama et al. 2006), suggest that Zn diffusion depth enhancement near the edge of diffusion apertures is likely. However, direct determination of such a depth variation has not been previously reported to our knowledge. Thus it is of interest to examine the Zn depth distribution in diffused planar APD structures, and determine the magnitude of variations in the photocurrent expected purely due to the junction edge curvature effect, compared to those associated with multiplication width variation associated with the Zn depth distribution.

In this work, the photocurrent distribution for a fully fabricated planar APD, processed using Zn diffusion, is reported. The Zn depth distribution is studied for diffused test structures using scanning electron microscopy (SEM) of both cross-sectional and plan-view samples. In order to simplify the analysis and obtain results representative of the junction curvature effect alone without any depth variation, the electric field and photocurrent distributions are simulated numerically for an InP/InGaAs APD without guard rings and with a single-step diffusion. The Zn dopant diffusion process is simulated numerically to generate realistic values for the junction curvature and the dopant concentration gradient near the junction. For simplicity, rather than implementing a model including diffusion depth variation across the device active area, the potential contribution of diffusion depth variations to the photocurrent variation is evaluated by comparing separate device simulations

with different values of the MW that are constant across the device. This allows for an analysis where the Zn depth is varied, while the edge effect contribution is held constant.

In section II, the numerical model is described in terms of process and device simulations using Technology Computer Aided Design tools by Silvaco (Santa Clara, CA, USA). In section III, the experimental characterization results are summarized to outline evidence in favor of a greater Zn diffusion depth along the active device edge. In section IV, the simulated electric field across the junction for a particular MW is simulated at breakdown for one particular MW to study the electric field distribution. Then, the current–voltage characteristics are simulated in the dark for three devices, each with a small variation in MW. A simulated beam of light is then rastered from the center to the edge of each device to study the photocurrent gain dependence on MW. Finally, conclusions are given on this study.

2 Numerical model

2.1 Epitaxial design and process simulation

The epitaxial structure of the APD is illustrated in Fig. 1, and consists of a separate absorption, grading, charge sheet and multiplication (SAGCM) configuration similar to Park et al. (2018); Pitts, et al. 2020). The simulated device radius is 30 microns with a Zn diffusion aperture of 15 microns, a single diffusion mask and no guard rings; the simulation assumes cylindrical coordinates. Three multiplication widths are explored: 1.0, 1.05 and 1.1 μm ; these values are intended to exaggerate an enhanced Zn diffusion depth of up to 100 nm. Note that the InP cap thickness is varied between 3.0 and 3.1 μm to maintain a constant diffusion depth for each MW explored; this ensures consistent edge field enhancement due to the curvature of the Zn diffusion profile.

The Athena module (v5.22.1.R) is adopted to simulate the diffusion of Zn through a SiN mask. The dopant species diffuses through InP via an interstitial-substitutional mechanism (Pitts et al. 2012; Tuck and Hooper 1975; Van Gorp et al. 1987). The Fermi model is used to simulate this process, since it assumes the defect population (In vacancies) is in thermodynamic equilibrium (Tuck and Hooper 1975), thus point defect-dopant pairs diffuse together based on the interstitial Zn diffusivity that is dependent on the dopant concentration (Tuck and Hooper 1975). The simulated diffusion profile was calibrated to secondary ion mass spectroscopy measurements of a large area Zn aperture with no charge sheet as illustrated in Fig. 2; the simulated data also include said charge sheet to highlight the MW within the non-intentionally

Fig. 1 Circularly symmetric APD simulation showing the layer structure and absolute doping concentration

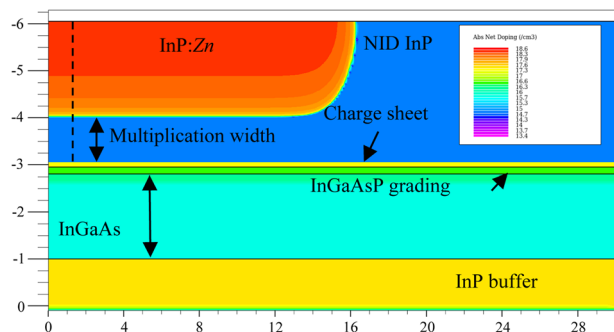
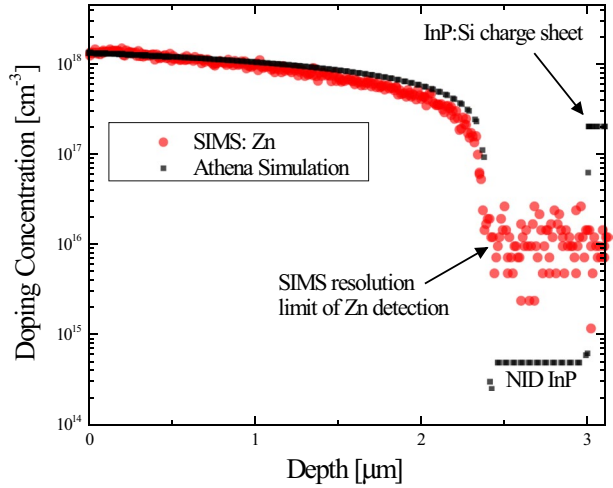


Fig. 2 Athena simulation of Zn diffusion compared to secondary ion mass spectroscopy measurements along cross-section; note the charge sheet is only included for the simulation in Athena



doped InP. Note the simulated edge of the Zn diffusion is ~ 50 nm shallower than the center in this diffusion model; in other words, there is no depth enhancement at the edges of the diffusion.

2.2 Device simulation

Prior to device simulation, the DevEdit tool (v2.8.26.R) is used to refine the mesh according to the dopant diffusion profile. This improves numerical accuracy of the electric field near the edge of the p - n junction. The Atlas tool (v5.23.12.C) then solves the partial differential equations that model semiconductor drift and diffusion in the structure using this mesh refinement. Recombination-generation rates are modeled using radiative, Shockley-Read-Hall and Auger processes (Walker and Denhoff 2017), impact ionization based on the Zappa model (Zappa, et al. 1996) and photogeneration rates using InGaAs optical properties based on a morphing algorithm using GaAs and InAs datasets (Schygulla et al. 2020); note that trap assisted tunneling and band to band tunneling are yet to be calibrated. Carrier mobilities are modeled using the dopant dependent carrier mobilities from Sotoodeh (Sotoodeh, et al. 2000). Also included is a surface leakage mechanism enabled through traps at the top InP surface to mimic experimental leakage currents.

First, the current voltage (I - V) simulation is performed until the compliance current (10 μ A) is reached to determine the breakdown voltage in the dark. Then, a beam of light (wavelength = 1.55 μ m, intensity = 0.05 W/cm²) is incident on the device from the front-side. A light I - V simulation is performed for a beam at the center, and then repeated as the beam is rastered across the device to beyond the junction edge. Due to cylindrical symmetry, the beam width is reduced as a function of distance from the center to maintain a constant generation rate in the InGaAs layer.

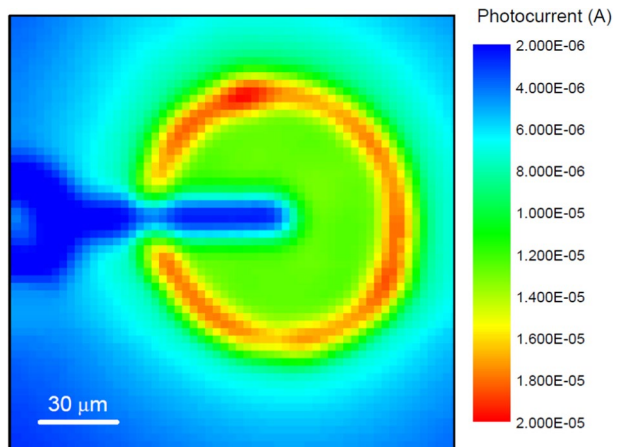
3 Experimental characterization

MOCVD-grown epi-wafers with the APD epitaxial structure described in section II-A were used for photocurrent rastering measurements and for scanning electron microscope (SEM) cross-section analysis. For the photocurrent rastering measurements, the wafers were fully processed into devices with a double Zn diffusion and Au-based metal contacts. The measurement used a 1.55 μm wavelength laser diode source, focused to a beam size of approximately 5 μm and rastered across the surface in a two-dimensional grid pattern. For these measurements, devices with a 15 μm wide centre contact were used, in order to obtain the photocurrent response around the edge of the device without metal shading effects. The cross-sectional SEM measurements were obtained from test wafers routinely used to calibrate the Zn diffusion depth, which are processed with a single Zn diffusion, then cleaved through the center of the diffusion apertures and imaged in the cleave plane.

Figure 3 shows a photocurrent raster map of an APD with two guard rings, fabricated using the double diffusion method. The bias point was set near the breakdown voltage, so as to obtain a dark current of 1 μA . The contact metallization is visible as a narrow (15 μm) finger of low response from the left side of the image to the device centre; the rest of the device is unshaded. The photocurrent map shows that the double diffusion method, in this case, does not completely suppress edge field enhancement effects, as an annulus of higher photocurrent due to enhanced gain is observed around the active area periphery. The peak value of the photocurrent near the edge is 20 μA , compared with 13 μA in the centre of the active area. While data for only one particular device are shown here, similar edge enhancement has been observed for devices with one, two or no guard rings, for several wafers fabricated using the same method, and at multiple locations on the wafers.

Figures 4a, b show SEM images of a cross section of a single-diffused test wafer. Due to the secondary electron contrast effect, the *p*-type Zn-diffused material in the top InP layer appears brighter in comparison with the *n*-type non-intentionally doped InP. Figure 4a was obtained from the center of the diffusion aperture, and Fig. 4b was obtained from the edge. The diffusion depth measured near the edge of the diffusion aperture is 1.862 μm , slightly deeper than the depth measured in the center of 1.832 μm . The difference of 0.03 μm corresponds to approximately 3 pixels at the original image resolution, limiting the precision with which the depth difference can be determined. The primary source of error in the

Fig. 3 Photocurrent map of an APD with two guard rings biased at breakdown; this device was fabricated using the double diffusion method. A 60% enhancement along the edge of the active device area compared to the center is observed



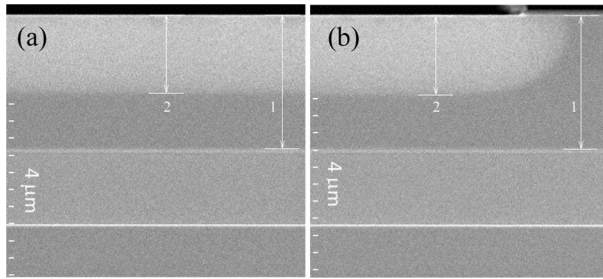


Fig. 4 Cross sectional SEM images of **a** the centre, and **b** the edge of a Zn-diffused aperture. The markers indicate the locations of extracted dimension measurements: The total InP thickness (marker 1) is $3.129\ \mu\text{m}$ in each case, while the Zn diffusion depth (marker 2) is $1.832\ \mu\text{m}$ in the centre of the aperture and $1.862\ \mu\text{m}$ near the edge

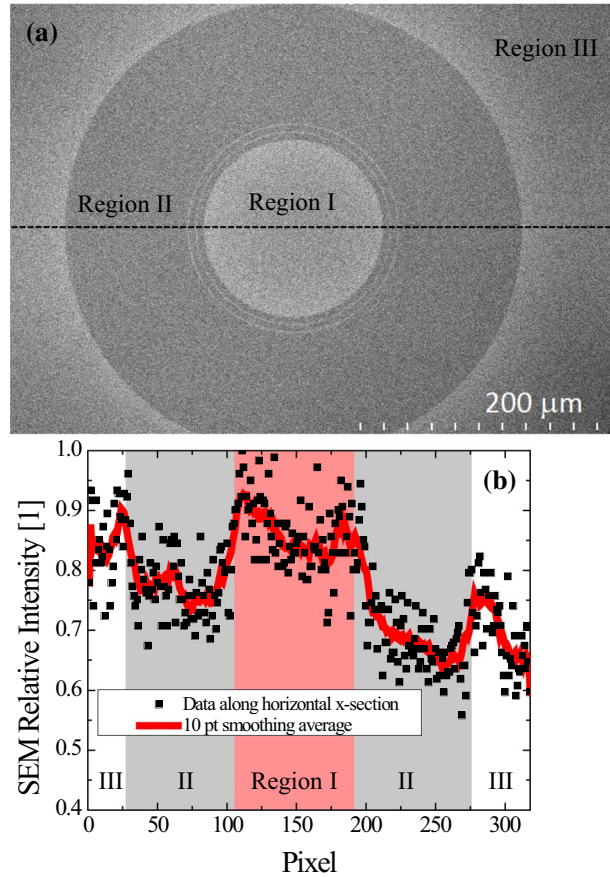
Zn depth measurement is in identifying the edge of the Zn diffusion, given the somewhat graded and indistinct transition in the brightness level in the images. A lower limiting value of the magnitude of this error can be estimated from the pixel size of the image, which is approximately $10\ \text{nm}$. Higher magnification settings did not allow for a higher precision measurement, since the edge of the Zn diffusion became more difficult to resolve due to reduced contrast.

The limited precision of the cross-sectional diffusion depth measurement motivated the development of a complementary technique which can identify regions of a relatively greater or smaller diffusion depth in the plane of the device, which can be readily compared with the photocurrent response map (Pitts, et al. 2020). In typical plan view SEM images of the surface of a Zn-diffused wafer, the Zn-diffused areas are easily distinguished due to the secondary electron contrast effect. However, such images cannot provide information on any variation in the Zn diffusion depth. Thus it is necessary to etch back the surface until contrast variations start to be visible due to the Zn-doped material being nearly completely removed in the areas with the least Zn depth. Since etching of around $2\ \mu\text{m}$ of material would not necessarily maintain the planarity of the surface, an etch stop was introduced to guarantee a planar starting surface.

A test epi-wafer was grown with $2\ \mu\text{m}$ of InP over a $25\ \text{nm}$ thick InGaAs etch stop layer. The wafer was patterned using the shallow diffusion mask of the APD device wafers, and then processed through a Zn diffusion targeting a depth of $2\ \mu\text{m}$ so as to place the p - n junction as close as possible to the etch stop layer. The diffusion mask was removed in buffered hydrofluoric acid, and the $2\ \mu\text{m}$ InP layer was selectively etched in an $\text{HCl}:\text{H}_3\text{PO}_4$ solution, stopping on the InGaAs layer. The InGaAs was then selectively removed in $1:5:50\ \text{H}_2\text{SO}_4:\text{H}_2\text{O}_2:\text{H}_2\text{O}$. Plan-view SEM images taken at this stage showed secondary electron contrast indicating the presence of p -type areas, without any marked difference from center to edge, thus confirming that Zn diffused to this depth. The InP below the etch stop is then etched back stepwise in short timed etches in $\text{HCl}:\text{H}_3\text{PO}_4$ solution, with SEM imaging performed at each step to check for contrast variations. In the case of the device studied in this work, such contrast variation from center to edge was observed after the first etch step, with approximately $70\ \text{nm}$ having been removed in a $5\ \text{s}$ etch time, and no further etching was performed.

A plan-view SEM image obtained after this etch is shown in Fig. 5a, outlining a center active device region with two guard rings (region I), a large masked annular

Fig. 5 **a** Plan view SEM image of a Zn-diffused test structure after etching to the plane of the p - n junction. **b** Pixel intensity along horizontal cross-section of **(a)**, where regions I, II and III are highlighted



region (II) and finally an unmasked outer region (III). The image shows a brighter band around the edge of the active device region (I), compared with its center, as well as a marked reduction in brightness in the far-field region III away from the outer edge of the circular masked area (region II), indicating that the etched surface is below the level of the p - n junction in that area. Although the magnitude of the depth variation cannot be determined from the plan-view image, it clearly shows the effect of mask loading on the Zn diffusion depth, with the depth decreasing away from the mask edge both in the device active area (region I) and the outer un-masked area (region III).

These results can also be observed in an intensity cross-section plot illustrated in Fig. 5b along the center; regions I–III are highlighted as bands. Since the data is noisy due to the contrast subtlety of the image, a 10-point smoothing average curve is included to highlight the relative enhancement along the edges between the regions. Comparing the center to the edge of Region I, a 10% enhancement can be observed. This is followed by a notable decrease in intensity in region II. Finally, the SEM intensity increases markedly entering into region III, before tailing off to the outer most parts of the image. This confirms that the Zn diffuses deeper into the structure along the edges of the mask. Again, no quantitative estimate of the depth enhancement can be extracted from this image.

The difference in depth obtained from the cross-sectional SEM images in Fig. 4 remains the best estimate of the magnitude of the depth variation from the center to the edge of the device for a single diffusion. Although SEM data on double diffused structures have so far not been obtained, it is reasonable to assume that both Zn diffusions are affected by similar edge enhancement effects, and therefore the depth variation from the center to the edge of the deep diffused active area is of similar magnitude as observed for the single diffusion.

4 Simulation results

4.1 Electric field near breakdown

First, the APD model is simulated to study the electric field distribution of the structure at breakdown. This is demonstrated for a device with $MW = 1 \mu\text{m}$ in Fig. 6a at $V = V_{BR}$, where V_{BR} is the breakdown voltage defined as the voltage when the dark current (I_D) reaches $10 \mu\text{A}$. An enhancement of the electric field is observed where the junction curvature begins at the edge of the diffusion aperture, with a peak field magnitude that is 2.7% higher than the maximum value in the centre. For comparison, a similar epitaxial stack with a $2 \mu\text{m}$ InP cap layer that also targets a $1 \mu\text{m}$ MW achieves a similar breakdown voltage, but showed a 27% enhancement of the maximum field at the edge compared to the center. This supports experimental findings that deeper Zn diffusion profiles exhibit lower edge breakdown behavior.

Fig. 6 **a** Simulated electric field distribution at device breakdown, and **b** cross-section of electric field at breakdown at various positions (center and across the Zn diffusion aperture)

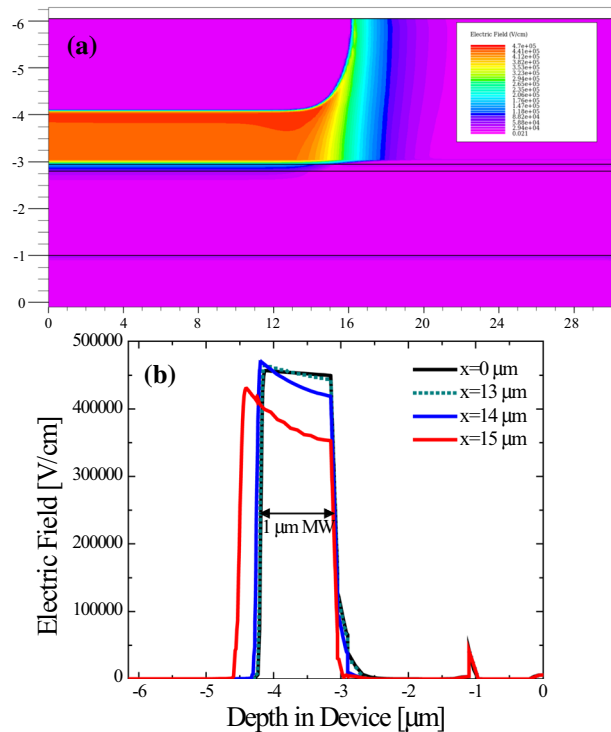


Figure 6b illustrates the electric field as a function of depth at the center and edge of the device corresponding to said breakdown voltage, which highlights the aforementioned peak electric field at the device edge. However, the integrated electric field across the MW is lower at the edge than at the center by $\sim 3.6\%$. Note that the MW is effectively wider at $x = 13 \mu\text{m}$ by $\sim 10 \text{ nm}$, by 70 nm at $x = 14 \mu\text{m}$, and finally by 300 nm at $x = 15 \mu\text{m}$. These results highlight the increased MW closer to the edge of the p - n junction, despite the higher electric field maximum close to breakdown.

4.2 Current–voltage simulation

Figure 7 illustrates the simulated current–voltage (I - V) of all three structures to compare the dark I - V and the light I - V corresponding solely to the centre beam ($x=0$). The magnitude of the dark current is similar between all structures due to the dominant surface leakage mechanism. Underlying this mechanism are radiative and SRH recombination until impact ionization dominates. The breakdown voltages range between -51.2 and -54.8 V , with a trend of 1.8 V per 50 nm increase in MW. The punch-through voltage has a similar trend for increasing MW. These features are in reasonable agreement to experimental measurements for a MW targeted for $1 \mu\text{m}$ (Pitts, et al. 2020). One major observation made from comparing the light I - V characteristics for the devices with different MWs is that for a fixed voltage (eg. $V = -50 \text{ V}$), a 50 nm decrease in MW results in a significantly enhanced gain. This is the main aspect of this simulation work that will be investigated further, with the assumption that this decreased MW is within the same device due to the mask loading effect (Pitts, et al. 2020).

The illuminated I - V characteristics resulting from a rastered beam for a device with $\text{MW} = 1 \mu\text{m}$ are illustrated in Fig. 8a, including a vertical line at -50 V . The inset is zoomed-in to illustrate the finer detail of the photocurrent simulation as a function of beam position. As the beam is rastered from the center of the device to beyond the edge of the junction ($x = 17 \mu\text{m}$), the photocurrent drops by approximately 7% . This will be investigated in more detail for all three devices at the same bias of -50 V , where the emphasis

Fig. 7 Simulated dark and illuminated current–voltage characteristics of all three devices of increasing MW, where the illuminating beam is incident at the center

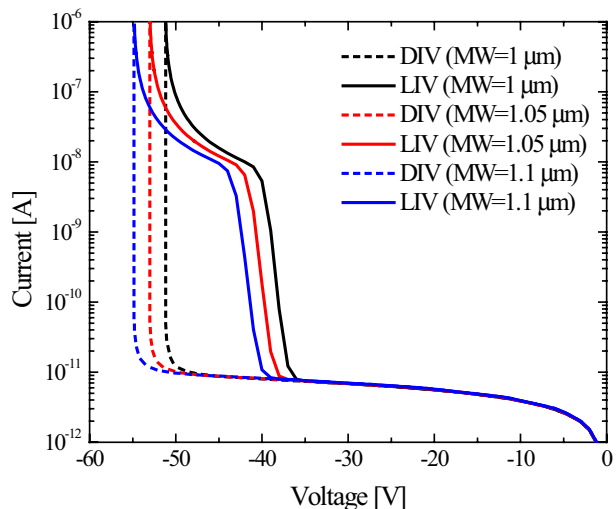
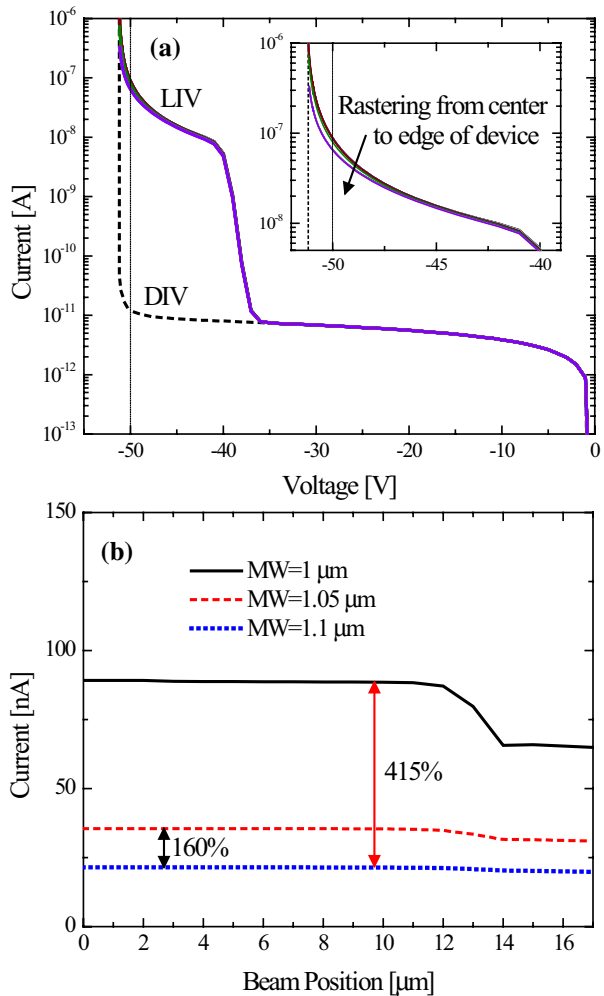


Fig. 8 a Simulated dark and illuminated current–voltage characteristics of a device with $MW = 1 \mu\text{m}$, where the beam is rastered from center to edge; inset shows zoomed in photocurrent variation from rastered beam including a vertical line at -50 V , and **b** the simulated photocurrent as a function of beam position for each MW device at a fixed bias of $V = -50 \text{ V}$



is placed on this variation in MW being within the same device rather than in separate devices as studied here.

Figure 8b shows the simulated photocurrent as a function of beam position for said bias of -50 V based on the three devices simulated. Beyond a beam position of $\sim 12 \mu\text{m}$, the photocurrent drops sharply for the device with a $MW = 1 \mu\text{m}$ (approximately 26%), consistent with the expected reduction in gain for the lower average field values in this region. The drop in photocurrent for larger MW devices is less sharp (as low as 7% for $MW = 1.1 \mu\text{m}$). It is worth noting that no increase in photocurrent occurs at the position $x = 14 \mu\text{m}$ at this bias, where the local peak in the electric field magnitude occurs, as shown in Fig. 2b. This is due to the gain being determined by the integrated, rather than peak value of the electric field. The simulation results suggest that for reasonably large diffusion depth – $2 \mu\text{m}$ is typically used and was simulated here – the electric field enhancement due to the junction curvature is likely not the origin of the observed photocurrent response increases near the edge, as reported for example in Burm et al. (2004); Theocharous et al. 2010).

Rather, for a fixed bias near the breakdown voltage, it can be observed that a fairly small change in the multiplication width can strongly enhance the photocurrent. For example, assuming a target MW = 1.1 μm , the photocurrent at $V = -50$ V is enhanced by 160% when the MW is reduced by only 50 nm, and 415% when the MW is reduced by 100 nm. The simulation results are in qualitative agreement with the observation in Pitts, et al. (2020) of enhanced photocurrent in areas of APD devices where the Zn diffusion depth was directly confirmed to be deeper, as well as the ring of enhanced photocurrent around the edge of the double-diffused device shown in Fig. 2, where the Zn diffusion depth is expected to be deeper based on the single-diffusion SEM results. Note that reduction in MW less than 50 nm is difficult to confirm accurately in experiment. Based on scanning electron microscopy images of cross-sectioned APDs, the reduction in MW could be as little as 30 nm. The simulation results from this analysis would still be indicative of a high sensitivity to such a small reduction in MW.

5 Conclusions

A planar avalanche photodiode structure with a single diffusion was simulated numerically. The maximum electric field obtained in the multiplication region at the edge is 2.7% higher than at the center. However, the model does not predict a higher photocurrent response at the device edge due to the junction curvature. Simulations performed with variations of the diffusion depth imply that a diffusion depth enhancement of 50 nm at the device edge would result in a photocurrent enhancement of 160% at a bias of $V = -50$ V, and up to 415% for a 100 nm diffusion depth enhancement. Overall, even a smaller enhancement < 50 nm would result in an appreciable increase in photocurrent near the edges. No significant photocurrent enhancement is reported as a result of junction curvature. Thus the mask loading effect must be well controlled to eliminate the impact of edge breakdown in planar APDs.

Acknowledgements This work was supported by the High Throughput and Secure Networks Challenge Program at the National Research Council of Canada. The authors would like to acknowledge G. Bonneville for his contribution to the photocurrent mapping measurements.

Funding Open Access provided by National Research Council Canada. The authors have not disclosed any funding.

Declarations

Conflict of interest The authors have no conflict of interest to declare that are relevant to the content of this article.

Open Access This article is licensed under a Creative Commons Attribution 4.0 International License, which permits use, sharing, adaptation, distribution and reproduction in any medium or format, as long as you give appropriate credit to the original author(s) and the source, provide a link to the Creative Commons licence, and indicate if changes were made. The images or other third party material in this article are included in the article's Creative Commons licence, unless indicated otherwise in a credit line to the material. If material is not included in the article's Creative Commons licence and your intended use is not permitted by statutory regulation or exceeds the permitted use, you will need to obtain permission directly from the copyright holder. To view a copy of this licence, visit <http://creativecommons.org/licenses/by/4.0/>.

References

- Anti, M., Acerbi, F., Tosi, A., Zappa, F.: 2D simulation for the impact of edge effects on the performance of planar InGaAs/InP SPADs. *Proc. Opt. Syst. Des. SPIE*. **8550**, 855025–855031 (2012). <https://doi.org/10.1117/12.2001704>
- Burm, J., et al.: Edge gain suppression of a planar-type InGaAs-InP avalanche photodiodes with thin multiplication layers for 10-Gb/s applications. *IEEE Photon. Technol. Lett.* **16**(7), 1721–1723 (2004). <https://doi.org/10.1109/LPT.2004.829546>
- Cho, S.R., et al.: Suppression of avalanche multiplication at the periphery of diffused junction by floating guard rings in a planar InGaAs-InP avalanche photodiode. *IEEE Photon Technol. Lett.* **12**(5), 534–536 (2000). <https://doi.org/10.1109/68.841277>
- Haralson, J.N., Parks, J.W., Brennan, K.F., Clark, W., Tarof, L.E.: Numerical simulation of avalanche breakdown within InP-InGaAs SAGCM standoff avalanche photodiodes. *J. Lightwave Technol.* **15**(11), 2137–2140 (1997). <https://doi.org/10.1109/50.641534>
- Li, B., et al.: Ultra low dark current, high responsivity and thin multiplication region in InGaAs/InP avalanche photodiodes. *Chin. Phys. Lett.* **29**(11), 118503 (2012). <https://doi.org/10.1088/0256-307X/29/11/118503>
- Liu, Y., et al.: A planar InP/InGaAs avalanche photodiode with floating guard ring and double diffused junction. *J. Lightwave Technol.* **10**(2), 182–193 (1992). <https://doi.org/10.1109/50.120573>
- Park, S.-H., et al.: Simulation studies on guard ring effects on edge breakdown suppression of InGaAs/InP avalanche photodiodes. *Jpn. J. Appl. Phys.* **57**(10), 106506 (2018). <https://doi.org/10.7567/JJAP.57.106506>
- Pitts, O.J., Benyon, W., Goodchild, D., Springthorpe, A.J.: Multiwafer Zn diffusion in an OMVPE reactor. *J. Cryst. Growth* **352**(1), 249–252 (2012). <https://doi.org/10.1016/j.jcrysgro.2011.10.006>
- Pitts, O.J et al.: Dopant depth distribution effects on the gain profile of avalanche photodiodes fabricated by Zn diffusion. *Novel Opt. Mater. Appl. pp NoTu2F-1*. (2020) <https://doi.org/10.1364/NOMA.2020.NoTu2F.1>
- Schygulla, P., Fuss-Kailuweit, P., Höhn, O., Dimroth, F.: Determination of the complex refractive index compound semiconductor alloys for optical device modeling. *J. Phys. D Appl. Phys.* **53**, 49 (2020). <https://doi.org/10.1088/1361-6463/abb270>
- Sotoodeh, M., et al.: Empirical low-field mobility model for III-V compounds applicable in device simulation codes. *J. Appl. Phys.* **87**(6), 2890–2900 (2000). <https://doi.org/10.1063/1.372274>
- Sugiyama, M., et al.: Control of abnormal edge growth in selective area MOVPE of InP. *J. Cryst. Growth* **287**(2), 668–672 (2006). <https://doi.org/10.1016/j.jcrysgro.2005.10.096>
- Theocharous, E., et al.: Characterization of the linearity of response and spatial uniformity of response of two InGaAsP/InP Geiger-mode avalanche photodiodes. *IEEE J. Quantum Electron.* **46**(11), 1561–1567 (2010). <https://doi.org/10.1109/JQE.2010.2053196>
- Tosi, A., Acerbi, F., Dalla Mora, A., Itzler, M.A., Jiang, X.: Active area uniformity of InGaAs/InP single-photon avalanche diodes. *IEEE Photon. J.* **3**(1), 31–41 (2010). <https://doi.org/10.1109/JPHOT.2010.2100037>
- Tuck, B., Hooper, A.: Diffusion profiles of zinc in indium phosphide. *J. Phys. D Appl. Phys.* **8**, 1806 (1975). <https://doi.org/10.1088/0022-3727/8/15/013>
- Van Gurp, G.J., Boudewijn, P.P.R., Kempeners, M.N.C., Tjaden, D.L.A.: Zinc diffusion in n-type indium phosphide. *J. Appl. Phys.* **61**(5), 1846–1855 (1987). <https://doi.org/10.1063/1.338028>
- Vasileuski, Y., et al.: Design considerations for guardring-free planar InGaAs/InP avalanche photodiode. *Opt. Quant. Electron.* **40**(14), 1247–1253 (2008). <https://doi.org/10.1007/s11082-009-9324-z>
- Walker, A.W., Denhoff, M.: Heavy and light hole minority carrier transport properties in low-doped n-InGaAs lattice matched to InP. *Appl. Phys. Lett.* **111**, 162107 (2017). <https://doi.org/10.1063/1.5002677>
- Wei, R., et al.: Optimization of 10-Gb/s long-wavelength floating guard ring InGaAs-InP avalanche photodiodes. *IEEE Photon Technol. Lett.* **14**(7), 977–979 (2002). <https://doi.org/10.1109/LPT.2002.1012404>
- Xiao, Y.G., Li, Z.Q., Simon Li, Z.M.: Suppressing premature edge breakdown for InP/InGaAs avalanche photodiodes by modeling analysis. *Proc SPIE 7055 Infrared Syst. Photoelectron. Technol. III* **70550**, 237–234 (2008). <https://doi.org/10.1117/12.795549>
- Zappa, F. et al.: Temperature dependence of electron and hole ionization coefficients in InP. In: Eighth International Conference Indium Phosphide and Related Materials, IPRM'96, Schwabisch Gmund, Germany April 21–25, pp. 628–631 (1996) <https://doi.org/10.1109/ICIPRM.1996.492327>